Since January 2020 Elsevier has created a COVID-19 resource centre with free information in English and Mandarin on the novel coronavirus COVID-19. The COVID-19 resource centre is hosted on Elsevier Connect, the company's public news and information website.

Cell Metabolism

Short Article

The Immunomodulatory Metabolite Itaconate Modifies NLRP3 and Inhibits Inflammasome Activation

Graphical Abstract

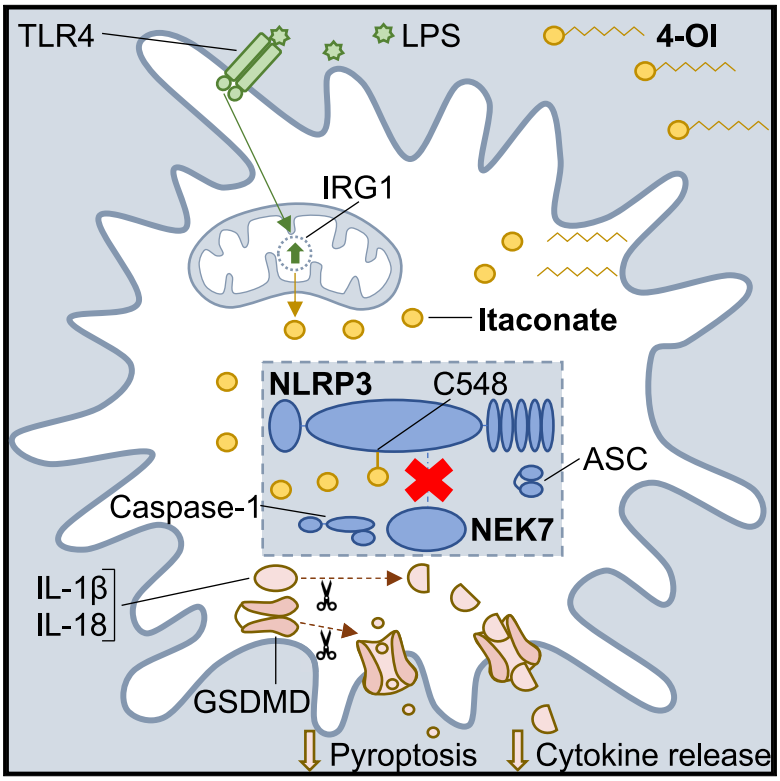

Highlights

- Itaconate and its derivative 4-OI (which generates itaconate) block NLRP3 activation
- Itaconate-depleted *Irg1*$^{-/-}$ BMDMs exhibit increased NLRP3 inflammasome activation
- 4-OI "dicarboxypropylates" C548 on NLRP3 and blocks the NLRP3-NEK7 interaction
- 4-OI reduces peritonitis *in vivo* and blocks IL-1β release from CAPS patient PBMCs

Authors

Alexander Hooftman, Stefano Angiari, Svenja Hester, ..., Alan D. Irvine, Roman Fischer, Luke A.J. O'Neill

Correspondence

laoneill@tcd.ie

In Brief

Hooftman et al. reveal a role for the Krebs cycle-derived metabolite itaconate in regulating the NLRP3 inflammasome. Itaconate specifically blocks NLRP3 inflammasome activation by reducing the NLRP3-NEK7 interaction, likely due to modification of C548 on NLRP3. Furthermore, itaconate inhibits IL-1β release from cells isolated from patients with the NLRP3-mediated disease CAPS.

Hooftman et al., 2020, Cell Metabolism *32*, 468–478
September 1, 2020
https://doi.org/10.1016/j.cmet.2020.07.016

CellPress

CellPress

Cell Metabolism

Short Article

The Immunomodulatory Metabolite Itaconate Modifies NLRP3 and Inhibits Inflammasome Activation

Alexander Hooftman,[1] Stefano Angiari,[1] Svenja Hester,[2] Sarah E. Corcoran,[1] Marah C. Runtsch,[1] Chris Ling,[3] Melanie C. Ruzek,[4] Peter F. Slivka,[4] Anne F. McGettrick,[1] Kathy Banahan,[1] Mark M. Hughes,[1] Alan D. Irvine,[5,6] Roman Fischer,[2] and Luke A.J. O'Neill[1,7,*]

[1]School of Biochemistry and Immunology, Trinity Biomedical Sciences Institute, Trinity College Dublin, Dublin 2, Ireland
[2]Nuffield Department of Medicine, Target Discovery Institute, University of Oxford, Oxford OX3 7FZ, UK
[3]Mass Spectrometry, Analytical Research Technologies, Abbvie, North Chicago, IL 60064, USA
[4]Immunology Discovery, Abbvie, Worcester, MA 01605, USA
[5]Pediatric Dermatology, Children's Health Ireland, Crumlin, Dublin 12, Ireland
[6]Clinical Medicine, Trinity College Dublin, Dublin 2, Ireland
[7]Lead Contact
*Correspondence: laoneill@tcd.ie
https://doi.org/10.1016/j.cmet.2020.07.016

SUMMARY

The Krebs cycle-derived metabolite itaconate is highly upregulated in inflammatory macrophages and exerts immunomodulatory effects through cysteine modifications on target proteins. The NLRP3 inflammasome, which cleaves IL-1β, IL-18, and gasdermin D, must be tightly regulated to avoid excessive inflammation. Here we provide evidence that itaconate modifies NLRP3 and inhibits inflammasome activation. Itaconate and its derivative, 4-octyl itaconate (4-OI), inhibited NLRP3 inflammasome activation, but not AIM2 or NLRC4. Conversely, NLRP3 activation was increased in itaconate-depleted *Irg1*$^{-/-}$ macrophages. 4-OI inhibited the interaction between NLRP3 and NEK7, a key step in the activation process, and "dicarboxypropylated" C548 on NLRP3. Furthermore, 4-OI inhibited NLRP3-dependent IL-1β release from PBMCs isolated from cryopyrin-associated periodic syndrome (CAPS) patients, and reduced inflammation in an *in vivo* model of urate-induced peritonitis. Our results identify itaconate as an endogenous metabolic regulator of the NLRP3 inflammasome and describe a process that may be exploited therapeutically to alleviate inflammation in NLRP3-driven disorders.

INTRODUCTION

Inflammasomes are intracellular multi-protein complexes that respond to a wide range of stimuli, including invading pathogens, host cell-derived danger signals, and environmental irritants (Lamkanfi and Dixit, 2014; Swanson et al., 2019). Numerous different inflammasomes exist, each responding to its own activating stimuli. The NOD-, LRR-, and pyrin domain-containing protein 3 (NLRP3) inflammasome is one of the best characterized inflammasomes, consisting of its central protein NLRP3, the adaptor protein ASC (also known as PYCARD), the mitotic kinase NIMA-related kinase 7 (NEK7) (He et al., 2016; Schmid-Burgk et al., 2016; Shi et al., 2016b), and the effector protein caspase-1. NLRP3 consists of three domains: an amino-terminal pyrin domain (PYD), a carboxy-terminal leucine-rich repeat (LRR) domain, and a central NACHT domain (Hu et al., 2013). Interactions between NLRP3 and NEK7 are essential for NLRP3 oligomerization and associated inflammasome activation, and these occur at multiple surfaces in the LRR and NACHT domains of NLRP3 (Sharif et al., 2019). Activation of the NLRP3 inflammasome results in caspase-1-mediated cleavage of pro-IL-1β, pro-IL-18, and gasdermin D into their active subunits. Despite advances in our understanding of the interactions that facilitate NLRP3 activation, a unifying molecular pathway from stimulus to NLRP3 activation remains to be elucidated. This is further complicated by the fact that the stimuli that trigger NLRP3 activation are so wide-ranging: potassium efflux (Muñoz-Planillo et al., 2013), chloride efflux (Domingo-Fernández et al., 2017; Tang et al., 2017), lysosomal disruption (Hornung et al., 2008), *trans*-Golgi network disassembly (Chen and Chen, 2018), and mitochondrial dysfunction (Groß et al., 2016; Shimada et al., 2012) are notable NLRP3-activating stimuli. The NLRP3 inflammasome may also be regulated metabolically. Mitochondrial localization of NLRP3 is thought to precede inflammasome activation (Iyer et al., 2013), and mitochondrial reactive oxygen species (ROS) have been implicated in NLRP3 activation (Groß et al., 2016). Furthermore, the ketone body β-hydroxybutyrate, produced as a result of a metabolic shift to fatty acid oxidation in conditions of low glucose, is an endogenous inhibitor of NLRP3 activation (Youm et al., 2015).

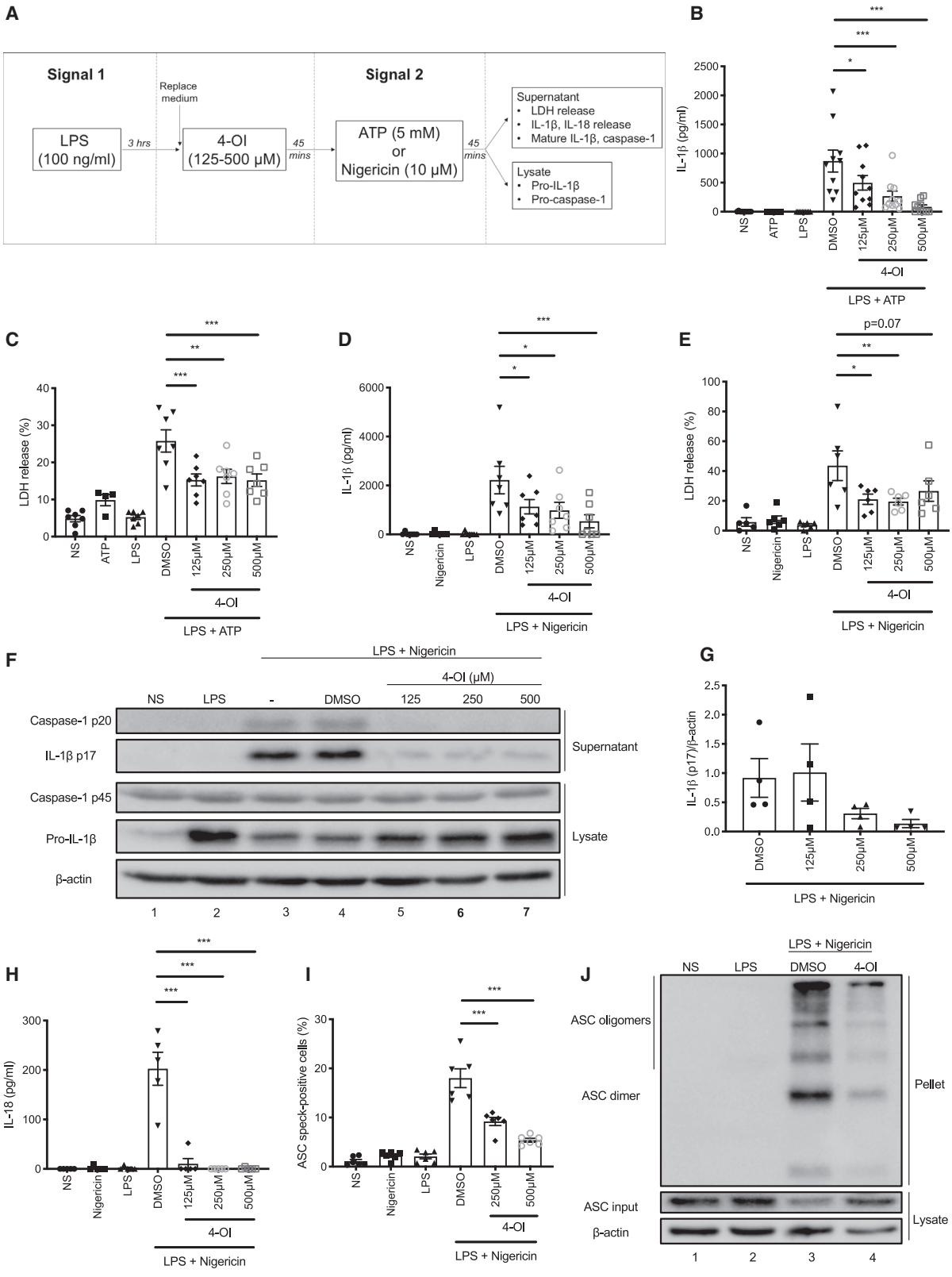

(legend on next page)

NLRP3 has been implicated in several diseases. Cryopyrin-associated periodic syndrome (CAPS) refers to a group of autoinflammatory disorders characterized by autosomal dominant mutations in *Nlrp3*, resulting in dysregulated release of IL-1β (Hoffman et al., 2001) and the development of multi-organ systemic inflammation. The role of NLRP3 in disease is not restricted to monogenic NLRP3-driven diseases, however, as NLRP3 has been implicated in a wide range of different autoinflammatory diseases including Alzheimer disease and rheumatoid arthritis (Mangan et al., 2018). The pathological involvement of NLRP3 therefore necessitates that its activation is tightly regulated. A major mechanism involves post-translational modifications. NLRP3 is ubiquitylated under resting conditions (Juliana et al., 2012), whereas its phosphorylation and acetylation promote activation (He et al., 2020; Stutz et al., 2017). Covalent inhibitors of NLRP3, which include parthenolide (Juliana et al., 2010) and oridonin (He et al., 2018), have revealed that NLRP3 is also susceptible to electrophilic modification of reactive cysteines, thus opening up another potential route through which NLRP3 inflammasome activation may be controlled.

Itaconate is an unsaturated dicarboxylic acid that is synthesized from the decarboxylation of the Krebs cycle intermediate *cis*-aconitate by the enzyme immune-responsive gene 1 (IRG1), also termed ACOD1 (Hooftman and O'Neill, 2019; Michelucci et al., 2013; O'Neill and Artyomov, 2019). Itaconate is a prime example of metabolic reprogramming in macrophages. Although synthesized as a by-product of the Krebs cycle, its production is scaled up upon LPS treatment (Lee et al., 1995) seemingly with the purpose of restraining macrophage immune responses to TLR stimulation. Endogenous itaconate and/or its cell-permeable derivative 4-octyl itaconate (4-OI) have been shown to alkylate cysteine residues on multiple proteins, including kelch-like ECH-associated protein 1 (KEAP1) (Mills et al., 2018), glyceraldehyde 3-phosphate dehydrogenase (GAPDH) (Liao et al., 2019), aldolase A (ALDOA) (Qin et al., 2019), and receptor-interacting serine/threonine-protein kinase 3 (RIPK3) (Qin et al., 2020). This form of cysteine alkylation, termed 2,3-dicarboxypropylation or itaconation, has been shown to be an important part of the anti-inflammatory properties of itaconate. As an example, the modification of KEAP1 activates the antioxidant transcription factor nuclear factor erythroid 2-related factor 2 (NRF2), thereby blocking macrophage IL-1β transcription following LPS stimulation, which requires ROS (Mills et al., 2018). However, the effect of itaconate on inflammasome-dependent IL-1β cleavage and release has not been fully explored. Here we provide evidence that itaconate modifies a specific cysteine (C548) on NLRP3 and inhibits NLRP3 activation by interfering with the interaction between NLRP3 and NEK7. Itaconate may therefore be an important negative regulator of NLRP3, which could have utility as a therapy in NLRP3-mediated diseases.

RESULTS

4-OI Specifically Blocks NLRP3 Inflammasome Activation

Treatment of LPS-primed bone marrow-derived macrophages (BMDMs) with 4-OI prior to activation of NLRP3 with ATP or nigericin (Figure 1A) resulted in a concentration-dependent reduction in IL-1β release (Figures 1B and 1D) as well as a reduction in LDH release (Figures 1C and 1E), which is used as a measure of pyroptosis. Cleavage and release of IL-1β in this assay were NLRP3-dependent (Figures S1A and S1B). The effect of 4-OI was confirmed by western blot as it blocked the cleavage of IL-1β and caspase-1 to their mature p17 and p20 forms, respectively (Figures 1F and 1G, compare lanes 5–7 to lane 4). 4-OI also blocked the cleavage of gasdermin D, the pyroptosis executioner (Shi et al., 2015), to its active N-terminal fragment (Figure S1C, compare lanes 5–7 to lane 4). Dimethyl itaconate (DMI), a different itaconate derivative, similarly blocked IL-1β release and cleavage (Figures S1D and S1E). However, the octyl control compounds 4-octyl succinate (4-OS) and 4-octyl-2-methyl succinate (4-O-2-MS), designed to control for the potentially reactive octyl tail on 4-OI, did not block IL-1β cleavage and release to the same extent (Figures S1F–S1H). The specific NLRP3 inhibitor MCC950 (Coll et al., 2015) was also used as a control in these experiments (Figures S1I and S1J). The cytokine IL-18 is co-secreted with IL-1β in an NLRP3-dependent manner (Ghayur et al., 1997), and its release was completely inhibited by 4-OI (Figure 1H). Upon NLRP3 inflammasome activation, the adaptor protein ASC is recruited by NLRP3 and forms large multimeric complexes (Lu et al., 2014), termed ASC specks. We found that 4-OI inhibited ASC speck formation, as detected by flow cytometry (Figure 1I), and reduced the appearance of large multimeric ASC complexes, as detected by western blot (Figure 1J, compare lane 4 to lane 3).

It was important to ensure that any effect was specific to NLRP3 activation rather than priming. We found that 4-OI did not affect tumor necrosis factor α (TNFα) release (Figure S2A) and only inhibited pro-IL-1β expression when added before LPS priming and not after LPS priming (Figure S2B, compare lanes 3–5 to lane 2 and lanes 7–9 to lane 6), in accordance with previous findings (Mills et al., 2018). In order to elucidate whether the effect was specific to the NLRP3 inflammasome, we also tested 4-OI in AIM2, NLRC4, and non-canonical inflammasome assays. 4-OI, when added between LPS and

Figure 1. 4-OI Blocks NLRP3 Inflammasome Activation

(A) Time flow of NLRP3 inflammasome assay with 4-OI in BMDMs.

(B and C) LPS (3 h) and ATP (45 min) induced IL-1β release (B, n = 10) and LDH release (C, n = 4 for ATP alone, n = 7 for others, measured as % LDH release of total lysis control) ± 4-OI.

(D and E) LPS (3 h) and nigericin (45 min) induced IL-1β release (D, n = 7) and LDH release (E, n = 5 for NS alone, n = 6 for others) ± 4-OI.

(F and G) Immunoblot analysis (F) and quantification by densitometry (G, n = 4) of pro- and mature caspase-1 and IL-1β protein in lysates and supernatants of BMDMs treated with LPS (3 h) and nigericin (45 min) ± 4-OI.

(H) LPS (3 h) and nigericin (45 min) induced IL-18 release ± 4-OI (n = 5).

(I) Percent of all cells positive for ASC specks in LPS- (3 h) and nigericin- (45 min) treated BMDMs ± 4-OI (n = 6).

(J) Immunoblot analysis of ASC protein in triton-insoluble pellet and -soluble lysate of LPS- (3 h) and nigericin- (45 min) treated BMDMs ± 4-OI (250 μM).

*p < 0.05, **p < 0.01, ***p < 0.001. Data are mean ± SEM. Blots are representative of a minimum of 3 independent experiments.

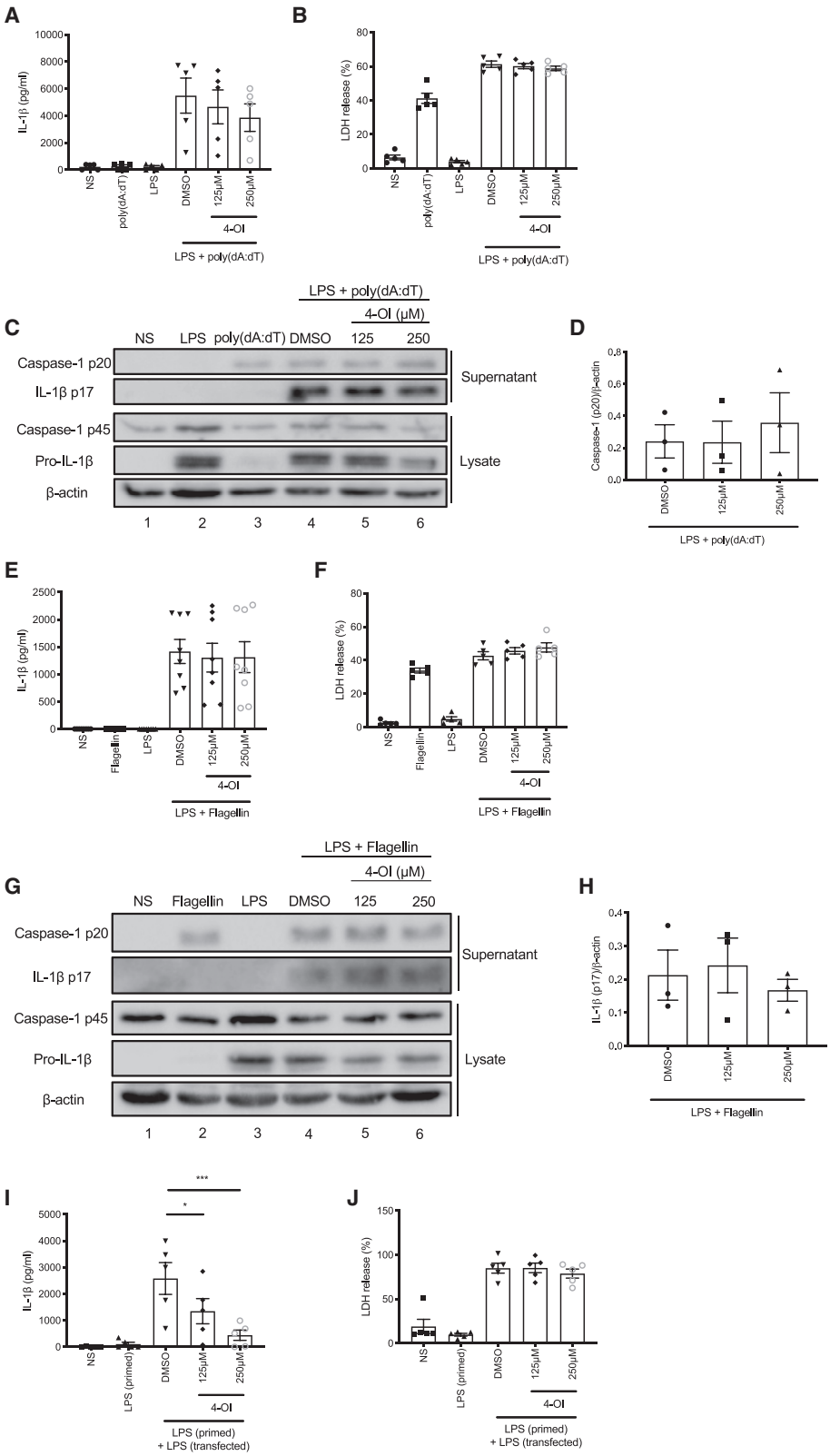

(legend on next page)

poly(dA:dT) transfection, did not reduce IL-1β release or pyroptosis associated with AIM2 inflammasome activation (Figures 2A and 2B). Furthermore, it had no effect on IL-1β or caspase-1 cleavage (Figures 2C and 2D, compare lanes 5 and 6 to lane 4). We made similar observations when 4-OI was added to cells between LPS and transfection of purified flagellin to activate the NLRC4 inflammasome. IL-1β release, pyroptosis, and cleavage of IL-1β and caspase-1 were unaffected by addition of 4-OI (Figures 2E–2H). The non-canonical inflammasome differs from canonical inflammasome signaling in that it senses cytosolic LPS using the effector protein caspase-11 (caspase-4 and -5 in humans) (Kayagaki et al., 2011; Shi et al., 2014). Although pyroptosis in this model is caspase-11 dependent, IL-1β release remains dependent on canonical NLRP3 activation, as this occurs secondary to K^+ efflux resulting from pyroptosis (Rathinam et al., 2019). We added 4-OI in between LPS priming and LPS transfection in a non-canonical inflammasome assay and found that it blocked IL-1β release, but not pyroptosis, in this assay, further indicating the specific targeting of NLRP3 (Figures 2I and 2J).

Endogenous Itaconate Regulates NLRP3 Inflammasome Activation

Although 4-OI treatment boosts levels of unmodified itaconate in activated macrophages (Mills et al., 2018), it is unclear whether LPS stimulation is required for this increase and whether the intracellular itaconate arises from de-esterification of 4-OI or from increased production of endogenous itaconate (Swain et al., 2020). We therefore examined whether 4-OI could directly generate itaconate. As shown in Figure S2C, $^{13}C_5$-labeled itaconate was detected in human macrophages treated with $^{13}C_5$ octyl itaconate both in the presence and absence of LPS. $^{13}C_5$ itaconate was detectable as soon as 30 min after treatment with $^{13}C_5$ octyl itaconate. This confirmed that 4-OI can indeed generate itaconate directly.

It is also unclear as to whether a transporter or cell-surface receptor exists for exogenous itaconate, hence the widespread use of itaconate derivatives in the field of itaconate biology. However, isotope tracing studies have shown that itaconate does accumulate in macrophages exposed to high concentrations of itaconic acid in culture media (Puchalska et al., 2018; Swain et al., 2020). Pre-treatment of BMDMs with itaconic acid (pH 7) prior to LPS and nigericin stimulation resulted in a significant and concentration-dependent reduction in IL-1β release (Figure S2E) and a non-significant reduction in pyroptosis (Figure S2F). Thus, unmodified itaconate, as well as derivatized itaconate, is capable of regulating NLRP3 activation.

The enzyme IRG1 is responsible for the production of itaconate in macrophages, which reaches a concentration of 5 mM in LPS-stimulated BMDMs (Mills et al., 2018). It is therefore possible to deplete or induce the production of endogenous itaconate through manipulation of IRG1. We performed NLRP3 inflammasome assays in *Irg1*$^{-/-}$ BMDMs and found that IL-1β release was significantly increased relative to wild-type (WT) BMDMs (Figure 3A). There was also a non-significant increase in pyroptosis in *Irg1*$^{-/-}$ BMDMs (Figure 3B). IL-1β and caspase-1 processing into their mature forms, as detected by western blot, was increased in *Irg1*$^{-/-}$ BMDMs (Figures 3C and 3D, compare lane 8 to lane 4). These effects were specific for NLRP3 inflammasome activation, as IL-1β release resulting from AIM2 inflammasome activation was not increased in *Irg1*$^{-/-}$ BMDMs (Figure S2G). As NLRP3 expression is LPS-inducible as part of priming, we verified that increased NLRP3 inflammasome activation in *Irg1*$^{-/-}$ BMDMs was not due to increased NLRP3 expression (Figure S2H, compare lane 4 to lane 2).

It is possible to reconstitute the murine NLRP3 inflammasome in HEK293T cells, as previously described (Shi et al., 2016a). Transfection of the various NLRP3 inflammasome components followed by stimulation with nigericin results in IL-1β cleavage and release from the cell (Figure 3E). We found that overexpression of a plasmid encoding IRG1 in this system resulted in reduced IL-1β cleavage and release relative to transfection of an empty vector plasmid (Figure 3E, compare lane 4 to lane 3). Thus, while the absence of endogenous itaconate boosts NLRP3 inflammasome activation, increased IRG1 expression has the opposite effect, indicating that endogenous itaconate regulates NLRP3.

4-OI Blocks the NLRP3-NEK7 Interaction and Dicarboxypropylates C548 on NLRP3

Itaconate alkylates C151 on KEAP1, in a modification termed 2,3-dicarboxypropylation (Mills et al., 2018), leading to activation of NRF2, a protein that is thought to regulate NLRP3 inflammasome activation (Garstkiewicz et al., 2017; Zhao et al., 2014). However, we found that 4-OI still inhibited NLRP3-dependent caspase-1 and IL-1β processing, as well as IL-1β release in *Nfe2l2*$^{-/-}$ (gene encoding NRF2) BMDMs (Figures S3A–S3D), ruling out NRF2 in the inhibitory process. Itaconate also limits inflammation through inhibition of succinate dehydrogenase (SDH) (Cordes et al., 2016; Lampropoulou et al., 2016). The SDH inhibitor dimethyl malonate (DMM), however, did not inhibit IL-1β release in an NLRP3 inflammasome assay (Figure S3E), indicating that SDH inhibition was unlikely to be important here. We also explored whether 4-OI may be interacting with the deglutathionylating enzyme glutathione transferase omega 1 (GSTO1-1), recently described as a regulator of NLRP3 inflammasome activation (Hughes et al., 2019). However, 4-OI still inhibited IL-1β release in an NLRP3 inflammasome assay in *Gsto1*$^{-/-}$ BMDMs (Figures S3F and S3G).

Figure 2. 4-OI Does Not Block Activation of Other Inflammasomes

(A and B) LPS (3 h) and poly(dA:dT) (6 h) induced IL-1β release (A, n = 5) and LDH release (B, n = 5) ± 4-OI.

(C and D) Immunoblot analysis (C) and quantification by densitometry (D, n = 3) of pro- and mature caspase-1 and IL-1β protein in lysates and supernatants of BMDMs treated with LPS (3 h) and poly(dA:dT) (6 h) ± 4-OI.

(E and F) LPS (3 h) and flagellin (2.5 h) induced IL-1β release (E, n = 8) and LDH release (F, n = 5) ± 4-OI.

(G and H) Immunoblot analysis (G) and quantification by densitometry (H, n = 3) of pro- and mature caspase-1 and IL-1β protein in lysates and supernatants of BMDMs treated with LPS (3 h) and flagellin (2.5 h) ± 4-OI.

(I and J) LPS priming (3 h) and transfection (18 h) induced IL-1β release (I, n = 5) and LDH release (J, n = 5) ± 4-OI.

*p < 0.05, **p < 0.01, ***p < 0.001. Data are mean ± SEM. Blots are representative of a minimum of 3 independent experiments.

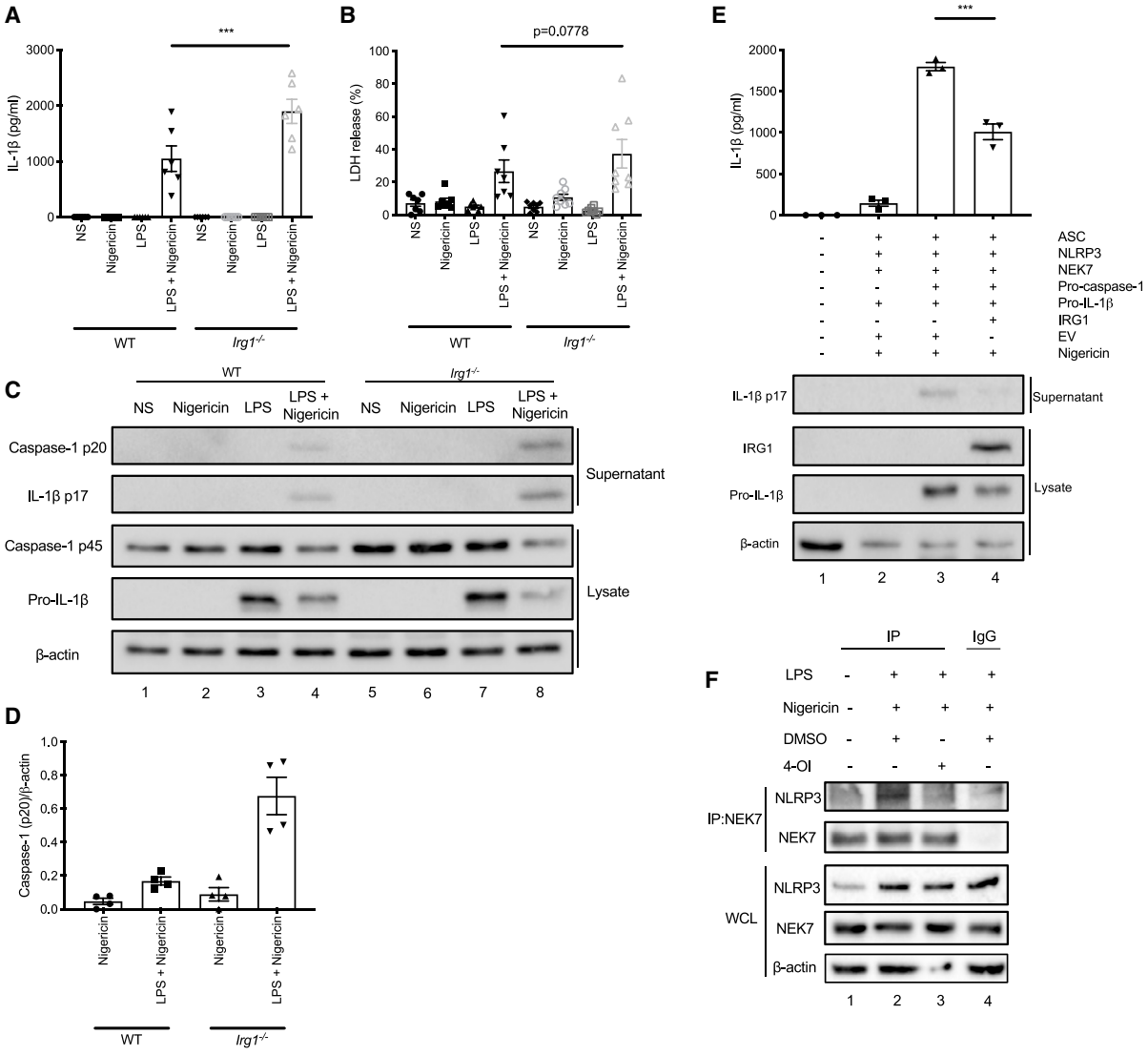

b ions	Sequence	*y* ions
98.06	P	
155.08	G	1618.84
212.10	G	1561.81
557.26	C(+242.15)	1504.79
644.27	S	1159.63
759.31	D	1072.61
872.39	L	957.59
985.47	L	844.50
1100.52	N(+.98)	731.40
1256.62	R	616.38
1371.65	D	460.28
1470.72	V	345.25
1598.81	K	246.18
	V	118.09

(legend on next page)

We subsequently hypothesized that the acute and specific effect of 4-OI on NLRP3 activation may be the result of targeting NLRP3 and/or NEK7 directly, but not ASC or caspase-1 as these components are shared by other inflammasomes. Upon NLRP3 inflammasome stimulation, NLRP3 and NEK7 interact with each other to promote activation (Sharif et al., 2019). This interaction was blocked by treatment with 4-OI (Figure 3F, compare lane 3 to lane 2). Subsequent tandem mass spectrometry of murine NLRP3, immunoprecipitated from 4-OI-treated NLRP3-overexpressing HEK293T cells, showed that 4-OI dicarboxypropylated (+242.15 Da) C548 on NLRP3 (Figure 3G). C548 is present in the helical domain 2 (HD2) of NLRP3, which is one of the surfaces at which NLRP3 interacts with NEK7 (Sharif et al., 2019). This points to a possible mechanism for inhibition of NLRP3, involving modification of NLRP3 on C548. This might interfere with the interaction between NLRP3 and NEK7, thereby blocking NLRP3 inflammasome activation.

4-OI Reduces NLRP3-Driven Peritonitis *In Vivo* and Blocks IL-1β Release from Human CAPS PBMCs

Monosodium urate (MSU) crystals, the causative agent of gout, are activators of the NLRP3 inflammasome and cause caspase-1- and ASC-dependent inflammation when injected into mice intraperitoneally (Martinon et al., 2006). Co-injection of 4-OI with MSU crystals reduced IL-1β and IL-6 (which is downstream of IL-1β) concentrations, as well as neutrophil numbers, in the peritoneal lavage fluid (Figures 4A–4C).

Finally, we tested 4-OI on peripheral blood mononuclear cells (PBMCs) from CAPS patients. We first confirmed that 4-OI would block NLRP3 activation in human PBMCs isolated from healthy donors. 4-OI, but not 4-O-2-MS, blocked IL-1β release when added between Pam3CSK4 or LPS and nigericin in human PBMCs (Figure 4D). 4-OI also blocked IL-1β cleavage into its mature form (Figures 4E and 4F, compare lane 5 to lane 4). The efficacy of 4-OI was similar to that of MCC950 and glyburide, albeit at a higher concentration (Figure S4A). PBMCs can also engage an "alternative" inflammasome pathway, which involves caspase-8 and NLRP3, and can be activated by LPS alone (Gaidt et al., 2016). 4-OI blocked IL-1β release from human PBMCs in this assay (Figure S4B). We then tested PBMCs isolated from the whole blood of CAPS patients who have hyperactive NLRP3, which can be stimulated with LPS to release large amounts of IL-1β. We treated CAPS PBMCs with 4-OI after 1 h stimulation with LPS and found that both 4-OI and MCC950 blocked IL-1β release from these cells (Figure 4G).

DISCUSSION

It is now generally accepted that NLRP3 inflammasome signaling plays a critical role in the pathogenesis of several autoimmune disorders, including Alzheimer disease (Heneka et al., 2013), rheumatoid arthritis (Vande Walle et al., 2014), and type 2 diabetes (Masters et al., 2010; Vandanmagsar et al., 2011). This has heightened the need for a greater understanding of how inflammasome activation is regulated endogenously and how it may be inhibited.

We hereby provide evidence of itaconate being a specific endogenous inhibitor of NLRP3 inflammasome activation. Previous studies have pointed toward a role for itaconate in regulating IL-1β cleavage (Lampropoulou et al., 2016; Swain et al., 2020), but by pre-treating cells with itaconate prior to LPS stimulation they were unable to rule out an effect on signal 1. Nor did these studies demonstrate itaconate's specificity for NLRP3, which we have shown through our AIM2 and NLRC4 experiments.

The mechanism that we propose for this inhibition is itaconate-mediated dicarboxypropylation of C548. This particular modification was also detected by Qin et al. using an itaconate-alkyne (iTALK) probe in Raw264.7 macrophages (Qin et al., 2020). It is possible that modification of NLRP3 at this surface would abolish its ability to interact with NEK7, a process that is necessary for inflammasome activation to take place (Sharif et al., 2019). However, further studies are required to establish (1) whether endogenous itaconate, as well as 4-OI, can cause the same modification—the study by Qin et al. indicates that this might be the case (Qin et al., 2020); (2) whether modification at this surface is functionally relevant with regard to inflammasome activation; and (3) whether there may be other targets for dicarboxypropylation along this pathway. Qin et al. also detected "itaconation sites" on gasdermin D, the pyroptosis executioner (Qin et al., 2020), further emphasizing the inhibitory effect of itaconate on pyroptosis. In addition, the recent observation that NEK7 deglutathionylation of C253 promotes NLRP3 inflammasome activation (Hughes et al., 2019) demonstrates that post-transcriptional modifications of NEK7 are also important in regulating inflammasome function.

Our observation that unmodified itaconic acid can limit NLRP3 activation is important when comparing the compounds widely used to deliver itaconate intracellularly. There has been a focus on how unmodified and derivatized itaconate diverge in their ability to accumulate inside the cell and exert immunomodulatory functions (Swain et al., 2020). However, we demonstrated that $^{13}C_5$-labeled octyl itaconate was converted into $^{13}C_5$ itaconate intracellularly and also found consistency in the way 4-OI and itaconic acid inhibited NLRP3 inflammasome activation. In contrast to the view of Swain et al. (2020), we feel that 4-OI can be used as a tool compound in the study of itaconate, since we have shown that it can be taken up and converted to intracellular itaconate by macrophages. We have previously also demonstrated that there is significant overlap in the cysteine

Figure 3. Endogenous Itaconate Regulates NLRP3 Activation and 4-OI Dicarboxypropylates C548 on NLRP3

(A and B) LPS (3 h) and nigericin (45 min) induced IL-1β release (A, n = 6) and LDH release (B) in wild-type (WT, n = 7) and *Irg1*$^{-/-}$ (n = 8) BMDMs.

(C and D) Immunoblot analysis (C) and quantification by densitometry (D, n = 4) of pro- and mature caspase-1 and IL-1β protein in lysates and supernatants of wild-type (WT) and *Irg1*$^{-/-}$ BMDMs treated with LPS (3 h) and nigericin (45 min).

(E) IL-1β release from NLRP3 inflammasome-reconstituted HEK293T cells treated with nigericin (45 min) (n = 3). Immunoblot analysis of pro- and mature IL-1β and IRG1 protein in supernatants and lysates of these cells.

(F) Endogenous co-immunoprecipitation of NLRP3 and NEK7 in BMDMs treated with LPS (3 h) and nigericin (45 min) ± 4-OI (250 μM).

(G) Tandem mass spectrometry spectrum of C548-containing NLRP3 peptide following 4-OI treatment (250 μM, 24 h).

*p < 0.05, **p < 0.01, ***p < 0.001. Data are mean ± SEM. Blots are representative of a minimum of 3 independent experiments.

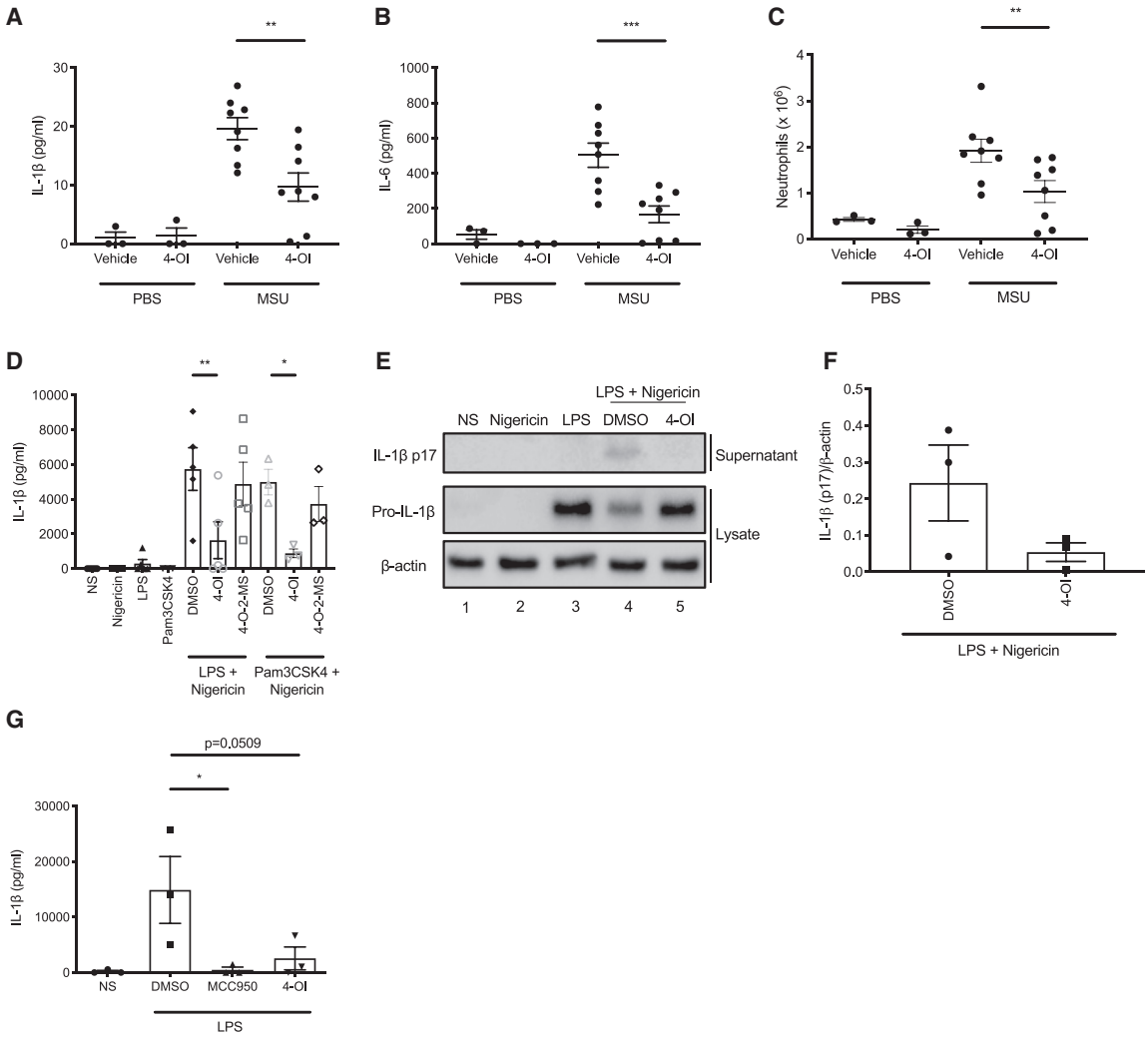

Figure 4. 4-OI Reduces Inflammation in a Murine *In Vivo* Model of Peritonitis and Blocks NLRP3 Inflammasome Activation in Healthy Human and CAPS PBMCs

(A–C) IL-1β concentration (A), IL-6 concentration (B), and neutrophil number (C) in the peritoneal lavage fluid of mice injected for 6 h with MSU crystals (30 mg/kg) ± 4-OI (50 mg/kg) (n = 3 for PBS groups, n = 8 for MSU groups).

(D) LPS or Pam3CSK4 (14 h) and nigericin (2 h) induced IL-1β release (n = 5 for LPS + nigericin, n = 3 for Pam3CSK4 + nigericin) ± 4-OI or 4-O-2-MS (both 250 μM) from healthy human PBMCs.

(E and F) Immunoblot analysis (E) and quantification by densitometry (F, n = 3) of pro- and mature IL-1β protein in lysates and supernatants of human PBMCs treated with LPS (14 h) and nigericin (2 h) ± 4-OI (250 μM).

(G) LPS (1 h) induced IL-1β release (n = 3) ± 4-OI (250 μM) or MCC950 (500 nM) from PBMCs isolated from CAPS patients.

*p < 0.05, **p < 0.01, ***p < 0.001. Data are mean ± SEM. Blots are representative of a minimum of 3 independent experiments.

residues alkylated by 4-OI and endogenous itaconate (Mills et al., 2018). In spite of this, it must be acknowledged that the relative electrophilicity of 4-OI/DMI, and therefore its ability to impact certain pathways (such as the ATF3-IKBζ axis), is higher than that of unmodified itaconate (Swain et al., 2020). As such, any results obtained with these derivatives must be verified in *Irg1*$^{-/-}$ experiments in order to be considered attributable to itaconate.

Our studies performed in *Irg1*$^{-/-}$ macrophages have shown that an absence of endogenous itaconate results in dysregulated IL-1β release and increased pyroptosis, establishing the importance of the itaconate-NLRP3 axis in restraining macrophage inflammation. Evidence suggests that, at least in the context of NLRP3 inflammasome activation, the presence of itaconate would limit pathogenic inflammation and resulting damage to the host. Recent studies showed that plasma itaconate levels correlated with improved disease score and reduced severity in patients with rheumatoid arthritis (Daly et al., 2020) and COVID-19 (Song et al., 2020), respectively. These studies add further weight to the concept that itaconate is a critical determinant of innate immune responses, with profound anti-inflammatory effects.

In conclusion, our work provides evidence for the regulation of NLRP3 by itaconate. Furthermore, in 4-OI we present a

compound that may be developed further for the treatment of NLRP3-driven disorders, as evidenced by its effect on IL-1β release from CAPS PBMCs. The targeting of NLRP3 by itaconate therefore holds tremendous therapeutic potential and expands the role of itaconate as a key immunometabolite that regulates innate immunity and inflammation.

Limitations of Study

Our study has demonstrated that 4-OI modifies C548 of NLRP3, a mechanism that is likely to be responsible for itaconate-mediated inhibition of inflammasome activation. However, further studies are required to demonstrate the functional effects of this modification, perhaps through site-directed mutagenesis of C548. Furthermore, the identification by Qin et al. of two additional cysteines undergoing modification, C284 and C720 (Qin et al., 2020), should also be functionally investigated. Qin et al. also uncovered modification of gasdermin D on C77 and C192 (Qin et al., 2020), which coupled with our results showing reduced gasdermin D cleavage with 4-OI, means that the effect of itaconate on gasdermin D should be examined. These studies should further emphasize the importance of the targeting of NLRP3-mediated pyroptosis as a key aspect of the anti-inflammatory effects of itaconate.

STAR★METHODS

Detailed methods are provided in the online version of this paper and include the following:

- KEY RESOURCES TABLE
- RESOURCE AVAILABILITY
  - Lead Contact
  - Materials Availability
  - Data and Code Availability
- EXPERIMENTAL MODEL AND SUBJECT DETAILS
  - Animal Details
  - Generation of Murine BMDMs
  - CAPS Patient Recruitment
  - Isolation of Human PBMCs
  - Human Monocyte Differentiation
  - Culture of HEK293T Cells
- METHOD DETAILS
  - Canonical Inflammasome Assays
  - Non-Canonical Inflammasome Assay
  - ASC Speck Assay
  - ASC Oligomerisation
  - HEK293T Inflammasome Reconstitution
  - Western Blotting
  - Co-Immunoprecipitation
  - ELISA
  - LDH Assay
  - Generation of $^{13}C_5$ Octyl Itaconate
  - Treatment of Human Macrophages with $^{13}C_5$ Octyl Itaconate
  - Measurement of $^{13}C_5$ Itaconate and $^{13}C_5$ Octyl Itaconate in Human Macrophages by LC-HRMS
  - Analysis of NLRP3 Modification by 4-OI
  - MSU-Induced Peritonitis Model
- QUANTIFICATION AND STATISTICAL ANALYSIS

SUPPLEMENTAL INFORMATION

Supplemental Information can be found online at https://doi.org/10.1016/j.cmet.2020.07.016.

ACKNOWLEDGMENTS

We thank Professor Richard Hartley (University of Glasgow) for synthesizing and supplying 4-OI, 4-OS, and 4-O-2-MS. We thank Professor Albena Dinkova-Kostova (University of Dundee) and Professor Ed Lavelle (Trinity College Dublin) for supplying bones from *Nfe2l2*$^{-/-}$ and *Nlrp3*$^{-/-}$ mice, respectively. We thank Dylan Ryan (University of Cambridge) for helpful discussions. The O'Neill laboratory acknowledges the following grant support: European Research Council Metabinate (834370), Science Foundation Ireland (12/IA/1531), and The Wellcome Trust (205455).

AUTHOR CONTRIBUTIONS

A.H. designed and performed experiments and analyzed the data. A.H. and L.A.J.O'N. wrote the manuscript. S.A. performed FACS analysis. S.A. and M.C.R. carried out *in vivo* experiments. S.H. and R.F. performed tandem mass spectrometry experiments. S.E.C. performed experiments on CAPS PBMCs, isolated from samples provided by A.D.I. C.L., M.C.R., and P.F.S. performed $^{13}C_5$ octyl itaconate experiments. K.B. generated plasmids for use in experiments. A.F.M. and M.M.H. assisted with experimental design. L.A.J.O'N. conceived ideas and oversaw the research program.

DECLARATION OF INTERESTS

The authors declare no competing interests.

Received: April 21, 2020
Revised: June 25, 2020
Accepted: July 28, 2020
Published: August 12, 2020

REFERENCES

Chen, J., and Chen, Z.J. (2018). PtdIns4P on dispersed trans-Golgi network mediates NLRP3 inflammasome activation. Nature *564*, 71–76.

Coll, R.C., Robertson, A.A., Chae, J.J., Higgins, S.C., Muñoz-Planillo, R., Inserra, M.C., Vetter, I., Dungan, L.S., Monks, B.G., Stutz, A., et al. (2015). A small-molecule inhibitor of the NLRP3 inflammasome for the treatment of inflammatory diseases. Nat. Med. *21*, 248–255.

Cordes, T., Wallace, M., Michelucci, A., Divakaruni, A.S., Sapcariu, S.C., Sousa, C., Koseki, H., Cabrales, P., Murphy, A.N., Hiller, K., and Metallo, C.M. (2016). Immunoresponsive gene 1 and itaconate inhibit succinate dehydrogenase to modulate intracellular succinate levels. J. Biol. Chem. *291*, 14274–14284.

Daly, R., Blackburn, G., Best, C., Goodyear, C.S., Mudaliar, M., Burgess, K., Stirling, A., Porter, D., McInnes, I.B., Barrett, M.P., and Dale, J. (2020). Changes in plasma itaconate elevation in early rheumatoid arthritis patients elucidates disease activity associated macrophage activation. Metabolites *10*, 241.

Domingo-Fernández, R., Coll, R.C., Kearney, J., Breit, S., and O'Neill, L.A.J. (2017). The intracellular chloride channel proteins CLIC1 and CLIC4 induce IL-1β transcription and activate the NLRP3 inflammasome. J. Biol. Chem. *292*, 12077–12087.

Gaidt, M.M., Ebert, T.S., Chauhan, D., Schmidt, T., Schmid-Burgk, J.L., Rapino, F., Robertson, A.A., Cooper, M.A., Graf, T., and Hornung, V. (2016). Human monocytes engage an alternative inflammasome pathway. Immunity *44*, 833–846.

Garstkiewicz, M., Strittmatter, G.E., Grossi, S., Sand, J., Fenini, G., Werner, S., French, L.E., and Beer, H.D. (2017). Opposing effects of Nrf2 and Nrf2-activating compounds on the NLRP3 inflammasome independent of Nrf2-mediated gene expression. Eur. J. Immunol. *47*, 806–817.

Ghayur, T., Banerjee, S., Hugunin, M., Butler, D., Herzog, L., Carter, A., Quintal, L., Sekut, L., Talanian, R., Paskind, M., et al. (1997). Caspase-1 processes IFN-gamma-inducing factor and regulates LPS-induced IFN-gamma production. Nature *386*, 619–623.

Groß, C.J., Mishra, R., Schneider, K.S., Médard, G., Wettmarshausen, J., Dittlein, D.C., Shi, H., Gorka, O., Koenig, P.A., Fromm, S., et al. (2016). K^+ efflux-independent NLRP3 inflammasome activation by small molecules targeting mitochondria. Immunity *45*, 761–773.

Han, J., Gagnon, S., Eckle, T., and Borchers, C.H. (2013). Metabolomic analysis of key central carbon metabolism carboxylic acids as their 3-nitrophenylhydrazones by UPLC/ESI-MS. Electrophoresis *34*, 2891–2900.

He, Y., Zeng, M.Y., Yang, D., Motro, B., and Núñez, G. (2016). NEK7 is an essential mediator of NLRP3 activation downstream of potassium efflux. Nature *530*, 354–357.

He, H., Jiang, H., Chen, Y., Ye, J., Wang, A., Wang, C., Liu, Q., Liang, G., Deng, X., Jiang, W., and Zhou, R. (2018). Oridonin is a covalent NLRP3 inhibitor with strong anti-inflammasome activity. Nat. Commun. *9*, 2550.

He, M., Chiang, H.H., Luo, H., Zheng, Z., Qiao, Q., Wang, L., Tan, M., Ohkubo, R., Mu, W.C., Zhao, S., et al. (2020). An acetylation switch of the NLRP3 inflammasome regulates aging-associated chronic inflammation and insulin resistance. Cell Metab. *31*, 580–591.e5.

Heneka, M.T., Kummer, M.P., Stutz, A., Delekate, A., Schwartz, S., Vieira-Saecker, A., Griep, A., Axt, D., Remus, A., Tzeng, T.C., et al. (2013). NLRP3 is activated in Alzheimer's disease and contributes to pathology in APP/PS1 mice. Nature *493*, 674–678.

Hoffman, H.M., Mueller, J.L., Broide, D.H., Wanderer, A.A., and Kolodner, R.D. (2001). Mutation of a new gene encoding a putative pyrin-like protein causes familial cold autoinflammatory syndrome and Muckle-Wells syndrome. Nat. Genet. *29*, 301–305.

Hooftman, A., and O'Neill, L.A.J. (2019). The immunomodulatory potential of the metabolite itaconate. Trends Immunol. *40*, 687–698.

Hornung, V., Ablasser, A., Charrel-Dennis, M., Bauernfeind, F., Horvath, G., Caffrey, D.R., Latz, E., and Fitzgerald, K.A. (2009). AIM2 recognizes cytosolic dsDNA and forms a caspase-1-activating inflammasome with ASC. Nature *458*, 514–518.

Hornung, V., Bauernfeind, F., Halle, A., Samstad, E.O., Kono, H., Rock, K.L., Fitzgerald, K.A., and Latz, E. (2008). Silica crystals and aluminum salts activate the NALP3 inflammasome through phagosomal destabilization. Nat. Immunol. *9*, 847–856.

Hu, Z., Yan, C., Liu, P., Huang, Z., Ma, R., Zhang, C., Wang, R., Zhang, Y., Martinon, F., Miao, D., et al. (2013). Crystal structure of NLRC4 reveals its autoinhibition mechanism. Science *341*, 172–175.

Hughes, M.M., Hooftman, A., Angiari, S., Tummala, P., Zaslona, Z., Runtsch, M.C., McGettrick, A.F., Sutton, C.E., Diskin, C., Rooke, M., et al. (2019). Glutathione transferase omega-1 regulates NLRP3 inflammasome activation through NEK7 deglutathionylation. Cell Rep. *29*, 151–161.e5.

Iyer, S.S., He, Q., Janczy, J.R., Elliott, E.I., Zhong, Z., Olivier, A.K., Sadler, J.J., Knepper-Adrian, V., Han, R., Qiao, L., et al. (2013). Mitochondrial cardiolipin is required for Nlrp3 inflammasome activation. Immunity *39*, 311–323.

Juliana, C., Fernandes-Alnemri, T., Wu, J., Datta, P., Solorzano, L., Yu, J.W., Meng, R., Quong, A.A., Latz, E., Scott, C.P., and Alnemri, E.S. (2010). Anti-inflammatory compounds parthenolide and Bay 11-7082 are direct inhibitors of the inflammasome. J. Biol. Chem. *285*, 9792–9802.

Juliana, C., Fernandes-Alnemri, T., Kang, S., Farias, A., Qin, F., and Alnemri, E.S. (2012). Non-transcriptional priming and deubiquitination regulate NLRP3 inflammasome activation. J. Biol. Chem. *287*, 36617–36622.

Kayagaki, N., Warming, S., Lamkanfi, M., Vande Walle, L., Louie, S., Dong, J., Newton, K., Qu, Y., Liu, J., Heldens, S., et al. (2011). Non-canonical inflammasome activation targets caspase-11. Nature *479*, 117–121.

Lamkanfi, M., and Dixit, V.M. (2014). Mechanisms and functions of inflammasomes. Cell *157*, 1013–1022.

Lampropoulou, V., Sergushichev, A., Bambouskova, M., Nair, S., Vincent, E.E., Loginicheva, E., Cervantes-Barragan, L., Ma, X., Huang, S.C., Griss, T., et al. (2016). Itaconate links inhibition of succinate dehydrogenase with macrophage metabolic remodeling and regulation of inflammation. Cell Metab. *24*, 158–166.

Lee, C.G., Jenkins, N.A., Gilbert, D.J., Copeland, N.G., and O'Brien, W.E. (1995). Cloning and analysis of gene regulation of a novel LPS-inducible cDNA. Immunogenetics *41*, 263–270.

Liao, S.T., Han, C., Xu, D.Q., Fu, X.W., Wang, J.S., and Kong, L.Y. (2019). 4-Octyl itaconate inhibits aerobic glycolysis by targeting GAPDH to exert anti-inflammatory effects. Nat. Commun. *10*, 5091.

Lu, A., Magupalli, V.G., Ruan, J., Yin, Q., Atianand, M.K., Vos, M.R., Schröder, G.F., Fitzgerald, K.A., Wu, H., and Egelman, E.H. (2014). Unified polymerization mechanism for the assembly of ASC-dependent inflammasomes. Cell *156*, 1193–1206.

Mangan, M.S.J., Olhava, E.J., Roush, W.R., Seidel, H.M., Glick, G.D., and Latz, E. (2018). Targeting the NLRP3 inflammasome in inflammatory diseases. Nat. Rev. Drug Discov. *17*, 688.

Martinon, F., Pétrilli, V., Mayor, A., Tardivel, A., and Tschopp, J. (2006). Gout-associated uric acid crystals activate the NALP3 inflammasome. Nature *440*, 237–241.

Masters, S.L., Dunne, A., Subramanian, S.L., Hull, R.L., Tannahill, G.M., Sharp, F.A., Becker, C., Franchi, L., Yoshihara, E., Chen, Z., et al. (2010). Activation of the NLRP3 inflammasome by islet amyloid polypeptide provides a mechanism for enhanced IL-1β in type 2 diabetes. Nat. Immunol. *11*, 897–904.

Michelucci, A., Cordes, T., Ghelfi, J., Pailot, A., Reiling, N., Goldmann, O., Binz, T., Wegner, A., Tallam, A., Rausell, A., et al. (2013). Immune-responsive gene 1 protein links metabolism to immunity by catalyzing itaconic acid production. Proc. Natl. Acad. Sci. USA *110*, 7820–7825.

Mills, E.L., Ryan, D.G., Prag, H.A., Dikovskaya, D., Menon, D., Zaslona, Z., Jedrychowski, M.P., Costa, A.S.H., Higgins, M., Hams, E., et al. (2018). Itaconate is an anti-inflammatory metabolite that activates Nrf2 via alkylation of KEAP1. Nature *556*, 113–117.

Muñoz-Planillo, R., Kuffa, P., Martínez-Colón, G., Smith, B.L., Rajendiran, T.M., and Núñez, G. (2013). K^+ efflux is the common trigger of NLRP3 inflammasome activation by bacterial toxins and particulate matter. Immunity *38*, 1142–1153.

O'Neill, L.A.J., and Artyomov, M.N. (2019). Itaconate: the poster child of metabolic reprogramming in macrophage function. Nat. Rev. Immunol. *19*, 273–281.

Puchalska, P., Huang, X., Martin, S.E., Han, X., Patti, G.J., and Crawford, P.A. (2018). Isotope tracing untargeted metabolomics reveals macrophage polarization-state-specific metabolic coordination across intracellular compartments. iScience *9*, 298–313.

Qin, W., Qin, K., Zhang, Y., Jia, W., Chen, Y., Cheng, B., Peng, L., Chen, N., Liu, Y., Zhou, W., et al. (2019). S-glycosylation-based cysteine profiling reveals regulation of glycolysis by itaconate. Nat. Chem. Biol. *15*, 983–991.

Qin, W., Zhang, Y., Tang, H., Liu, D., Chen, Y., Liu, Y., and Wang, C. (2020). Chemoproteomic profiling of itaconation by bioorthogonal probes in inflammatory macrophages. J. Am. Chem. Soc. *142*, 10894–10898.

Rathinam, V.A.K., Zhao, Y., and Shao, F. (2019). Innate immunity to intracellular LPS. Nat. Immunol. *20*, 527–533.

Richard, J.-V., Delaite, C., Riess, G., and Schuller, A.-S. (2016). A comparative study of the thermal properties of homologous series of crystallisable n-alkyl maleate and itaconate monoesters. Thermochim. Acta *623*, 136–143.

Schmid-Burgk, J.L., Chauhan, D., Schmidt, T., Ebert, T.S., Reinhardt, J., Endl, E., and Hornung, V. (2016). A genome-wide CRISPR (clustered regularly interspaced short palindromic repeats) screen identifies NEK7 as an essential component of NLRP3 inflammasome activation. J. Biol. Chem. *291*, 103–109.

Sharif, H., Wang, L., Wang, W.L., Magupalli, V.G., Andreeva, L., Qiao, Q., Hauenstein, A.V., Wu, Z., Núñez, G., Mao, Y., and Wu, H. (2019). Structural mechanism for NEK7-licensed activation of NLRP3 inflammasome. Nature *570*, 338–343.

Shi, J., Zhao, Y., Wang, Y., Gao, W., Ding, J., Li, P., Hu, L., and Shao, F. (2014). Inflammatory caspases are innate immune receptors for intracellular LPS. Nature *514*, 187–192.

Shi, J., Zhao, Y., Wang, K., Shi, X., Wang, Y., Huang, H., Zhuang, Y., Cai, T., Wang, F., and Shao, F. (2015). Cleavage of GSDMD by inflammatory caspases determines pyroptotic cell death. Nature *526*, 660–665.

Shi, H., Murray, A., and Beutler, B. (2016a). Reconstruction of the mouse inflammasome system in HEK293T cells. Bio Protoc. *6*, 1–10.

Shi, H., Wang, Y., Li, X., Zhan, X., Tang, M., Fina, M., Su, L., Pratt, D., Bu, C.H., Hildebrand, S., et al. (2016b). NLRP3 activation and mitosis are mutually exclusive events coordinated by NEK7, a new inflammasome component. Nat. Immunol. *17*, 250–258.

Shimada, K., Crother, T.R., Karlin, J., Dagvadorj, J., Chiba, N., Chen, S., Ramanujan, V.K., Wolf, A.J., Vergnes, L., Ojcius, D.M., et al. (2012). Oxidized mitochondrial DNA activates the NLRP3 inflammasome during apoptosis. Immunity *36*, 401–414.

Song, J.W., Lam, S.M., Fan, X., Cao, W.J., Wang, S.Y., Tian, H., Chua, G.H., Zhang, C., Meng, F.P., Xu, Z., et al. (2020). Omics-driven systems interrogation of metabolic dysregulation in COVID-19 pathogenesis. Cell Metab. *32*, 188–202.

Stutz, A., Kolbe, C.C., Stahl, R., Horvath, G.L., Franklin, B.S., van Ray, O., Brinkschulte, R., Geyer, M., Meissner, F., and Latz, E. (2017). NLRP3 inflammasome assembly is regulated by phosphorylation of the pyrin domain. J. Exp. Med. *214*, 1725–1736.

Swain, A., Bambouskova, M., Kim, H., Andhey, P.S., Duncan, D., Auclair, K., Chubukov, V., Simons, D.M., Roddy, T.P., Stewart, K.M., and Artyomov, M.N. (2020). Comparative evaluation of itaconate and its derivatives reveals divergent inflammasome and type I interferon regulation in macrophages. Nat Metab *2*, 594–602.

Swanson, K.V., Deng, M., and Ting, J.P. (2019). The NLRP3 inflammasome: molecular activation and regulation to therapeutics. Nat. Rev. Immunol. *19*, 477–489.

Tang, T., Lang, X., Xu, C., Wang, X., Gong, T., Yang, Y., Cui, J., Bai, L., Wang, J., Jiang, W., and Zhou, R. (2017). CLICs-dependent chloride efflux is an essential and proximal upstream event for NLRP3 inflammasome activation. Nat. Commun. *8*, 202.

Vandanmagsar, B., Youm, Y.H., Ravussin, A., Galgani, J.E., Stadler, K., Mynatt, R.L., Ravussin, E., Stephens, J.M., and Dixit, V.D. (2011). The NLRP3 inflammasome instigates obesity-induced inflammation and insulin resistance. Nat. Med. *17*, 179–188.

Vande Walle, L., Van Opdenbosch, N., Jacques, P., Fossoul, A., Verheugen, E., Vogel, P., Beyaert, R., Elewaut, D., Kanneganti, T.D., van Loo, G., and Lamkanfi, M. (2014). Negative regulation of the NLRP3 inflammasome by A20 protects against arthritis. Nature *512*, 69–73.

Youm, Y.H., Nguyen, K.Y., Grant, R.W., Goldberg, E.L., Bodogai, M., Kim, D., D'Agostino, D., Planavsky, N., Lupfer, C., Kanneganti, T.D., et al. (2015). The ketone metabolite β-hydroxybutyrate blocks NLRP3 inflammasome-mediated inflammatory disease. Nat. Med. *21*, 263–269.

Zhao, C., Gillette, D.D., Li, X., Zhang, Z., and Wen, H. (2014). Nuclear factor E2-related factor-2 (Nrf2) is required for NLRP3 and AIM2 inflammasome activation. J. Biol. Chem. *289*, 17020–17029.

STAR★METHODS

KEY RESOURCES TABLE

REAGENT or RESOURCE	SOURCE	IDENTIFIER
Antibodies		
Anti-β-actin	Sigma	Cat# A5316; RRID: AB_476743
Anti-ASC	Santa Cruz	Cat# Sc-22514-r; RRID: AB_2174874
Anti-Caspase-1	Adipogen	Cat# AG-20B-0042-C100; RRID: AB_2755041
Anti-CD11b eFluor 660	Invitrogen	Cat# 50-0112-82; RRID: AB_11218507
Anti-CD16/CD32	Biolegend	Cat# 101302; RRID: AB_312801
Anti-CD45 APC/Cy7	Biolegend	Cat# 103116; RRID: AB_312981
Anti-FLAG	Sigma	Cat# F1804; RRID: AB_262044
Anti-GSDMD	Sigma	Cat# G7422; RRID: AB_1850381
Anti-GSTO1-1	Genetex	Cat# GTX118439; RRID: AB_11174551
Anti-HA	Sigma	Cat# H3663; RRID: AB_262051
Anti-IL-1β	R&D	Cat# AF-401-NA; RRID: AB_416684
Anti-IL-1β (Human)	R&D	Cat# AF-201-NA; RRID: AB_354387
Anti-IRG1	Abcam	Cat# AB222411
Anti-Ly6G	Biolegend	Cat# 127611; RRID: AB_1877212
Anti-NEK7	Abcam	Cat# AB133514
Anti-NLRP3	Cell Signaling	Cat# D4D8T; RRID: AB_2722591
Anti-NRF2	Cell Signaling	Cat# 12721S; RRID: AB_2715528
Anti-Rabbit IgG Alexa Fluor 488	Invitrogen	Cat# A-11008; RRID: AB_143165
Rabbit IgG	Merck	Cat# PP64; RRID: AB_97852
Chemicals, Peptides, and Recombinant Proteins		
4-Octyl Itaconate	Professor Richard Hartley, University of Glasgow	Cat# N/A
4-Octyl Succinate	Professor Richard Hartley, University of Glasgow	Cat# N/A
4-Octyl-2-Methyl Succinate	Professor Richard Hartley, University of Glasgow	Cat# N/A
A/G PLUS Agarose Beads	Santa Cruz	Cat# sc-2003
ATP	Invivogen	Cat# tlrl-atpl
Coomassie Blue R-250	Cayman	Cat# 14500
Disuccinimidyl Suberate	ThermoFisher	Cat# 21655
Elastase	Promega	Cat# V1891
FuGENE HD Transfection Reagent	Promega	Cat# E2311
Itaconic Acid	Sigma	Cat# I29204
Lipofectamine 2000	ThermoFisher	Cat# 11668030
LPS from *E.coli* O127:B8	Sigma	Cat# L5668
Lymphoprep	StemCell Technologies, Inc.	Cat# 07861
Monosodium Urate Crystals	Invivogen	Cat# tlrl-msu
Nigericin	Invivogen	Cat# tlrl-nig
Pam3SCK4	Invivogen	Cat# tlrl-pms
Poly (dA:dT)	Invivogen	Cat# tlrl-patn
Purified Flagellin from *P.aeruginosa*	Invivogen	Cat# tlrl-pafla
Recombinant Human M-CSF	Peprotech	Cat# 300-25
Strataclean Resin	Agilent Technologies	Cat# 400714

(*Continued on next page*)

Continued

REAGENT or RESOURCE	SOURCE	IDENTIFIER
Ultrapure rough LPS from *E. coli*, serotype EH100	Enzo	Cat# ALX-581-010-L001
Zombie Green Fixable Viability Kit	Biolegend	Cat# 423111
Critical Commercial Assays		
Cytotox 96 non-radioactive cytotoxicity assay	Promega	Cat# G1780
Human IL-1β DuoSet ELISA	R&D Systems	Cat# DY201
Mouse IL-1β DuoSet ELISA	R&D Systems	Cat# DY401
Mouse IL-1β Quantikine ELISA	R&D Systems	Cat# MLB00C
Mouse IL-18 ELISA	Invitrogen	Cat# BMS618-3
Mouse IL-6 DuoSet ELISA	R&D Systems	Cat# DY406
Mouse TNFα DuoSet ELISA	R&D Systems	Cat# DY410
Experimental Models: Cell Lines		
Human: HEK293T cells	Sigma	Cat# 12022001
Experimental Models: Organisms/Strains		
Mouse: C57BL/6	Harlan	N/A
Mouse: C57BL/6N-Acod1$^{em1(IMPC)J}$/J	Jackson	Cat# 029340
Mouse: GSTO1-1$^{-/-}$ 129/SvEv-C57BL/6	Taconic	Cat# TF1210
Recombinant DNA		
FLAG-NLRP3	Shi et al., 2016b	Addgene; Cat# 75127
FLAG-Pro-Caspase-1	Shi et al., 2016b	Addgene; Cat# 75128
FLAG-pro-IL-1β	Shi et al., 2016b	Addgene; Cat# 75131
GFP-IRG1	Origene	Cat# MG217265
HA-ASC	Hornung et al., 2009	Addgene; Cat# 41553
HA-NEK7	Shi et al., 2016b	Addgene; Cat# 75142
Software and Algorithms		
FlowJo v 10.7	FlowJo	https://www.flowjo.com/solutions/flowjo
Graphpad Prism 8.0	Graphpad	https://www.graphpad.com/
Image Lab 6.1	Bio-Rad	https://www.bio-rad.com
PEAKS Studio 8	Bioinformatics Solutions	https://www.bioinfor.com/peaks-studio/

RESOURCE AVAILABILITY

Lead Contact

Further information and requests for resources and reagents should be directed to and will be fulfilled by the Lead Contact, Luke A.J. O'Neill (laoneill@tcd.ie).

Materials Availability

This study did not generate new unique reagents.

Data and Code Availability

This study did not generate/analyze datasets/code.

EXPERIMENTAL MODEL AND SUBJECT DETAILS

Animal Details

All mice were on a C57BL/6J background unless stated below. Wild-type mice were purchased from Harlan. *Irg1*$^{-/-}$ mice (named C57BL/6N-Acod1$^{em1(IMPC)J}$/J) were generated by CRISPR-targeted deletion of exon 4 of *Acod1*, and were purchased from The Jackson Laboratory. Wild-type littermates were used as controls. *Gsto1*$^{-/-}$ 129/SvEv-C57BL/6J mice were obtained from Taconic and were originally derived from 129S-5 ES cells and backcrossed to an albino C57BL/6J strain. Bones from *Nfe2l2*$^{-/-}$ mice and their wild-type counterparts were kindly provided by Professor Albena Dinkova-Kostova (University of Dundee). Bones from *Nlrp3*$^{-/-}$

mice and their wild-type counterparts were kindly provided by Professor Ed Lavelle (Trinity College Dublin). *In vivo* models were performed with 6-week old female C57BL/6J mice and littermates were randomly assigned to experimental groups. Animals were maintained under specific pathogen-free conditions in line with Irish and European Union regulations. All animal procedures were ethically approved by the Trinity College Dublin Animal Research Ethics Committee prior to experimentation, and conformed with the Directive 2010/63/EU of the European Parliament.

Generation of Murine BMDMs

6-12-week old mice were euthanised in a CO_2 chamber, and death was confirmed by cervical dislocation. Bone marrow was subsequently harvested from the tibia and fibula and cells were differentiated in DMEM containing L929 supernatant (10%), fetal calf serum (FCS) (10%), and penicillin/streptomycin (1%) for 6 days, after which cells were counted and plated at 0.5×10^6 cells/mL unless otherwise stated.

CAPS Patient Recruitment

Recruitment was carried out by members of the patient's own clinical team. Patients were approached to provide a voluntary blood sample for the study. Patients were provided with an information leaflet 24 h in advance of sample donation. All patients or their parents/legal guardians gave informed written consent. Direct travel costs were covered but no incentive or compensation was offered. Patient demographics were not recorded. Patients were receiving standard anti-IL-1 therapy (Anakinra). This treatment was not discontinued prior to blood sampling. The study was conducted in accordance with the Declaration of Helsinki and approved by the Joint Research Ethics Committee of St James Hospital and Tallaght Hospital (REF 2017-11) and the Ethics (Medical Research) Committee of Our Lady's Children's Hospital, Crumlin (Now Children's Health Ireland), REF: GEN/577/17.

Isolation of Human PBMCs

Human blood samples from healthy donors were collected and processed at the School of Biochemistry and Immunology in TBSI (TCD). Blood samples were obtained anonymously and written informed consent for the use of blood for research purposes has been obtained from the donors. All the procedures involving experiments on human samples have been approved by the School of Biochemistry and Immunology Research Ethics Committee (TCD). Experiments were conducted according to the TCD guide on good research practice, which follows the guidelines detailed in the National Institutes of Health Belmont Report (1978) and the Declaration of Helsinki.

30 mL whole blood was layered on 20 mL Lymphoprep (Axis-Shield), followed by centrifugation for 20 min at 400 x g with the brake off, after which the upper plasma layer was removed and discarded. The layer of mononuclear cells at the plasma-density gradient medium interface was retained, and 20 mL PBS was added. Cells were centrifuged for 8 min at 300 x g and the resulting supernatant was removed and discarded. The remaining pellet of mononuclear cells was resuspended, counted and plated at 1×10^6 cells/mL in RPMI supplemented with FCS (10%) and penicillin-streptomycin (1%).

Human Monocyte Differentiation

Frozen human monocytes (Biological Specialty Labs) were thawed and seeded in 10 cm dishes at 1×10^6 cells/mL in macrophage media (RPMI media supplemented with 10% fetal calf serum and penicillin/streptomycin) and 0.1 μg/mL recombinant human M-CSF (Peprotech) and incubated at 37°C and 5% CO2. Cells were cultured for 6 days total to differentiate the monocytes to macrophages, with removal and replacement of media and M-CSF at three days of culture.

Culture of HEK293T Cells

HEK293T cells were obtained from the Centre for Applied Microbiology and Research (Wiltshire, UK) and cultured in DMEM containing FCS (10%) and penicillin-streptomycin (1%).

METHOD DETAILS

Canonical Inflammasome Assays

BMDMs were plated in 12-well cell culture plates and left overnight to adhere. Cells were treated the following day with LPS from *Escherichia coli*, serotype EH100 (Enzo Life Sciences, 100 ng/mL) for 3 h. Medium was removed and replaced with serum- and antibiotic-free medium and treated with compounds as required for 45 min. 4-OI, 4-O-2-MS and 4-OS were kindly supplied by Professor Richard Hartley and dissolved in DMSO. Itaconic acid (Sigma Aldrich) was dissolved at 500 mM in PBS and the required volume of NaOH was added in order to achieve a pH of 7. Cells were treated with nigericin (10 μM, Invivogen) or ATP (5 mM, Sigma Aldrich) for 45 min to activate the NLRP3 inflammasome. In order to activate the AIM2 inflammasome, LPS-primed cells were transfected with 1.5 μg poly(dA:dT) (Invivogen) using lipofectamine 2000 (Thermo Fisher Scientific) for 6 h. In order to activate the NLRC4 inflammasome, LPS-primed cells were transfected with 1.6 μg purified flagellin from *Pseudomonas aeruginosa* (Invivogen) for 2.5 h.

To activate the NLRP3 inflammasome in healthy human PBMCs, cells were treated for 14 h with LPS (200 ng/mL) or Pam3CSK4 (2 μg/mL, Invivogen). Medium was removed and replaced with serum- and antibiotic-free medium and treated with compounds as required for 45 min. Cells were subsequently treated with nigericin (6.5 μM) for 2 h. For alternative inflammasome activation in healthy human PBMCs, cells were pre-treated with compounds for 1 h, after which they were treated with LPS (200 ng/mL) for 14 h, as

described previously (Gaidt et al., 2016). Human CAPS PBMCs were treated for 1 h with LPS (100 ng/mL), after which medium was removed and replaced with serum- and antibiotic-free medium and treated with compounds as required for 4 h.

Non-Canonical Inflammasome Assay

Cells were treated with LPS (100 ng/mL) for 3 h, after which the medium was replaced and cells were treated with compounds as required for 45 min. 2 μg LPS was transfected using FuGENE HD (Promega) overnight (18 h) in order to activate the inflammasome.

ASC Speck Assay

Flow cytometry was used to analyze ASC speck formation following inflammasome activation. BMDMs were treated as desired, after which the supernatant was removed and 1 mL of cold PBS was added to the wells. Cells were then detached from the plates using a cell scraper and transferred to round-bottom tubes. 4 mL ethanol (100%) was added to the cells while simultaneously vortexing the tubes, in order to fix the cells and prevent clumping. Cells were incubated at room temperature for 15 min, before being centrifuged at 600 x g for 10 min. Supernatant was removed, and cells were resuspended in FACS buffer (0.1% Sodium azide, 0.1% BSA, 1.5% FCS in PBS) containing FC block (0.4%). Cells were incubated for 20 min at room temperature after which anti-mouse ASC antibody (Santa Cruz, sc-22514-R) was added to a final dilution of 1/1500. Cells were incubated for 90 min at room temperature. 1 mL of FACS buffer was added to the cells and they were centrifuged at 600 x g for 10 min. Supernatant was removed, and the cells were resuspended in Alexa Fluor 488 anti-rabbit IgG antibody (Invitrogen, A27304 1/1500 in FACS buffer), before being incubated in the dark for 45 min at room temperature. Cells were pelleted and resuspended in 200 μL FACS buffer. Samples were acquired on a FACSCanto (BD Biosciences). Samples were gated based on forward light scatter (FSC) versus side scatter (SSC) in order to exclude cell debris. Doublets were also excluded from analysis using FSC-area versus FSC-width analysis. Sorting was conducted by analyzing the pulse height, width and area of the 488nm laser and 530/30nm laser channel. ASC speck positive cells were detected by a decreased width or increased height in the pulse of emitted fluorescence when compared with unstimulated cells.

ASC Oligomerisation

BMDMs were treated as desired. After treatment, cells were washed twice with 200 μL cold PBS before being lysed in crosslinking lysis buffer (50 mM HEPES, 0.5% Triton X-100, 1 mM phenylmethylsulfonyl fluoride (PMSF), 11.5 μg/mL aprotinin, 1 μg/mL leupeptin and 1 mM sodium orthovanadate). Samples were placed on ice for 15 min and benzonase nuclease was added in order to break down DNA in the lysates. Lysates were centrifuged for 15 min at 6000 x g at 4°C and the supernatant was removed and frozen down as the 'soluble fraction.' 20 μL of the soluble fraction was mixed with 5 μL of sample lysis buffer (0.125M Tris pH 6.8, 10% glycerol, 0.02% SDS, 5% DTT) and run on a 12% gel. The insoluble pellet was resuspended in HEPES (50 mM) and washed 3 times by centrifuging at 6000 x g at 4°C and removing the supernatant each time. After the final wash, the pellet was resuspended in 500 μL crosslinking buffer (50 mM HEPES, 150 mM NaCl) and disuccinimidyl suberate (DSS, Thermo Fisher, made up in anhydrous DMSO) was added to the final concentration of 2 mM. Immediately following the addition of DSS, the sample was inverted several times and incubated for 45 min at 37°C. The sample was then centrifuged for 15 min at 6000 x g at 4°C, before the supernatant was removed and the pellet was resuspended in 30 μL sample lysis buffer. The resuspended 'insoluble fraction' was subsequently boiled for 5 min at 95°C before being run on a gel.

HEK293T Inflammasome Reconstitution

HEK293T cells were plated at a density of 2×10^5 cells/mL in 24-well plates in DMEM containing FCS (10%). The following morning, cells were transfected with plasmids encoding murine GFP-IRG1 (280 ng, Origene, MG217265) and murine NLRP3 inflammasome components: HA-ASC (20 ng, Addgene, 41553), HA-NEK7 (200 ng, Addgene, 75142), FLAG-pro-caspase 1 (100 ng, Addgene, 75128), FLAG-NLRP3 (200 ng, Addgene, 75127), FLAG-Pro-IL-1β (200 ng, Addgene, 75131). Plasmids were transfected using lipofectamine 2000 for 24 h. Following the 24 h transfection, medium was replaced with DMEM containing FCS (10%) and penicillin-streptomycin (1%). 4 h later, nigericin (10 μM) was added to cells in order to activate the inflammasome. Supernatants and cell lysates were harvested 45 min later. This protocol was described previously (Shi et al., 2016a).

Western Blotting

Supernatant was removed from cells following stimulation and lysates were harvested in 30-50 μL lysis buffer (0.125 M Tris pH 6.8, 10% glycerol, 0.02% SDS, 5% DTT) Lysates were subsequently heated to 95°C for 5 min to denature proteins. In order to concentrate supernatants for western blot, 5 μL Strataclean Resin (Agilent) was added to 500 μL of supernatant and vortexed for 1 min. Supernatants were then centrifuged at 210 x g for 2 min at 4°C. Supernatants were removed and discarded, and the remaining pellet was resuspended in 30 μL lysis buffer. SDS-PAGE was used to resolve proteins by molecular weight. Samples were boiled at 95°C for 5 min prior to loading into a 5% stacking gel. The percentage resolving gel depended on the molecular weight of the given protein. The Bio-Rad gel running system was used to resolve proteins and the Bio-Rad wet transfer system was used for the electrophoretic transfer of proteins onto PVDF membrane. Following transfer, the membrane was incubated in milk powder (5% in TBST) for 1 h and subsequently incubated in primary antibody rolling overnight at 4°C. The membrane was incubated for 1 h with secondary antibody (diluted in 5% milk powder) at room temperature. Prior to visualization, the membrane was immersed in WesternBright ECL Spray (Advansta). Protein visualization took place on a ChemiDoc MPTM Imaging System (Bio-Rad), and both chemiluminescent and white light images were taken. Quantification of western blot images was performed using Image Lab Software (Bio-Rad). Adjusted band

volume was calculated for each band and for each experimental condition this was presented as target protein/housekeeping protein.

Co-Immunoprecipitation

BMDMs were seeded at $1x10^6$ cells/mL in 10 cm dishes the day prior to treatment. The following day, cells were treated as required. Following treatment, cells were washed with 3 mL PBS before lysis in 500 μL low stringency lysis buffer (50 mM HEPES pH 7.5, 100 mM NaCl, 1 mM EDTA, 10% glycerol, 0.5% Nonident P40 (NP-40), 1 mM phenylmethylsulfonyl fluoride (PMSF), 11.5 μg/mL aprotinin, 1 μg/mL leupeptin and 1 mM sodium orthovanadate) on ice. Plates were scraped with a cell scraper and lysate transferred into microcentrifuge tubes. Tubes were agitated at 1100 rpm at 4°C for 15 min before being centrifuged at 21380 x g for 10 min at 4°C. 25 μL of resulting supernatant was mixed with 25 μL sample lysis buffer and treated as the whole cell lysate (WCL) sample. 0.0153 mg/mL anti-NEK7 antibody (Abcam, ab133514) or the equivalent concentration of rabbit IgG antibody (Millipore, pp64), and 40 μL A/G PLUS agarose beads (Santa Cruz) was added to the remaining supernatant, which was subsequently incubated at 4°C in a ferris wheel mixer for 3 h. IP samples were subsequently centrifuged at 400 x g for 2 min at 4°C, supernatant removed, and beads washed three times with 1 mL low stringency lysis buffer. The immune complexes were eluted by addition of 40 μL sample lysis buffer, boiled for 5 min and analyzed by SDS-PAGE.

ELISA

DuoSet ELISA kits for IL-1β, TNFα and IL-6 were purchased from R&D Systems and were carried out according to the manufacturer's instructions with appropriately diluted cell supernatants added to each plate in duplicate or triplicate. Quantikine ELISA kits for IL-1β (R&D Systems) and IL-18 (Invitrogen) were similarly carried out according to the manufacturer's instructions. Absorbance at 450 nm was then quantified using a FLUOstar Optima plate reader. Corrected absorbance values were calculated by subtracting the background absorbance, and cytokine concentrations were subsequently obtained by extrapolation from a standard curve plotted on GraphPad Prism 8.0.

LDH Assay

The CytoTox 96 Non-Radioactive Cytotoxicity Assay (Promega) was used to quantify lactate dehydrogenase (LDH) release from cells as a measure of cell death in BMDMs following inflammasome stimulation. Freshly harvested supernatants were used in this assay. 50 μL of each supernatant was added to 50 μL Cytotox 96 Reagent and incubated in the dark at room temperature for 30 min. 50 μL acetic acid was added to stop the reaction, and the absorbance at 492 nm was measured using a FLUOstar optima. 100 μL total lysis solution was added to untreated cells 30 min before harvesting and served as a maximum LDH release control. Medium alone was also used to correct for background absorbance.

Generation of $^{13}C_5$ Octyl Itaconate

All NMR spectra were collected using a Varian 400 MHz NMR. Synthesis was performed by WuXi AppTec. Synthesis of $^{13}C_5$ octyl itaconate was performed as previously described (Richard et al., 2016) with minor modifications. Uniformly labeled $^{13}C_6$-citric acid (0.32 mmol) was placed into a distillation apparatus and subjected to pyrolysis by heating to 175°C for 30 min with constant stirring. The reaction was then heated up to 200°C at a pressure of 2 Torr. Heating was maintained for 2 h. The cyclised product was collected as a white solid in the distillation bulb at a temperature of −20°C (3.9% yield). Equimolar quantities of the product and octanol (20 mM final concentration) were mixed in toluene, heated to 100°C and stirred for 12 h. The mixture was concentrated and subjected to preparative HPLC using a Shimadzu LC-8A preparative HPLC with a Waters Xbridge column (150 mm x 25 mm, 5 μM). Mobile phase consisted of 10 mM ammonium bicarbonate in water with a gradient of acetonitrile from 15% to 45% over 20 min with a flow rate of 30 mL/min. Purified yield of $^{13}C_5$-octylitaconate was 20%. Synthesis of $^{13}C_5$-octylitaconate was confirmed by ^{1}H NMR and LC/MS (ESI+).

Treatment of Human Macrophages with $^{13}C_5$ Octyl Itaconate

At the end of the macrophage differentiation, medium was removed and replaced with macrophage medium with or without 100 ng/mL of LPS, from *Escherichia coli* serotype O127:B8 (Sigma) and 125 μM $^{13}C_5$ octyl itaconate dissolved in DMSO and incubated for various times at 37°C and 5% CO2. In cultures with $^{13}C_5$ octyl itaconate alone, supernatants and cells were harvested 0.5, 3, 6, 9 and 27 h after addition of $^{13}C_5$ octyl itaconate. Cultures with LPS were treated with $^{13}C_5$ octyl itaconate three h prior or three h following LPS addition. Supernatants and cells were harvested 3, 6 and 24 h post LPS if added after $^{13}C_5$ octyl itaconate and 6, 9 and 24 h post LPS if added before $^{13}C_5$ octyl itaconate. Control cultures without $^{13}C_5$ octyl itaconate included cells alone and 24 h treatment with LPS. Supernatants were transferred to Eppendorf tubes and stored at −80°C until analysis. Cells were washed with D-PBS (GIBCO), trypsinized (GIBCO), scraped with a cell scraper and transferred to conical tubes. Cells were washed three times with 40 mM ammonium formate (Sigma) and transferred to Eppendorf tubes prior to snap freezing on dry ice and stored at −80°C until analysis.

Measurement of $^{13}C_5$ Itaconate and $^{13}C_5$ Octyl Itaconate in Human Macrophages by LC-HRMS

Cell pellet samples were thawed on wet ice immediately prior to analysis. 1 mL of ice cold 8:2 methanol-water (Sigma; Milli-Q water) was added to each sample. The tubes were briefly vortexed, sonicated (10 min/ice bath), and briefly vortexed again to lyse cells and extract analytes. Each sample was centrifuged at 6°C for 15 min at 15,000 x g. 450 μL of supernatant was transferred to a 1.5 mL

glass autosampler vial, dried down, and derivatized with 3-nitrophenylhydrazine (3-NPH) (Sigma) using a modification of method previously reported method (Han et al., 2013). 100 μL of a 250 mM 3-NPH solution (1:1 acetonitrile-water) and 200 μL of a 143.5 mM EDC.HCl solution (1:1 water:acetonitrile containing 6%(v/v) pyridine) were added to each vial. The samples were briefly vortexed and left at room temperature for 2 h. After adding 500 μL chloroform (Sigma) and 100μL of cold 3N HCl (VWR) each vial was vortexed for about 5 s, and the layers were allowed to separate. 450 μL of the lower organic layer was transferred to a Microsolv Max Recovery 1.2 mL glass vial and dried down. The residue was reconstituted in 100 μL of methanol-water (1:1) for analysis by LC-HRMS.

The LC-HRMS system consisted of an Agilent 1290 HPLC system coupled to an Agilent 6550 Q-TOF mass spectrometer equipped with a Jet Stream ESI source. The chromatographic analysis was performed with a Waters Acquity BEH C18 column (100 × 2.1 mm, 1.7 μm) maintained at 35°C and an elution gradient composed of water (A) and acetonitrile (B). The gradient elution profile was 0.5% B for 2 min, 90% B at 20 min, 90% B to 28 min with column re-equilibration at 0.5% B from 28.05 to 33 min. The flow rate was 0.35 mL/min and the injection volume was 3 μL. The mass spectrometer was operated in negative ion mode with the following source settings: Gas Temp: 290°C, Drying Gas: 12 L/min, Nebulizer: 55 psi, Sheath Gas Temp: 400°C, Sheath Gas Flow: 12, Vcap: 3000V, Nozzle: 1000V. Acquisition rate: 1.5 spectra/s.

Analysis of NLRP3 Modification by 4-OI

HEK293T cells were plated at a density of 3 × 10^5 cells/mL in 10 cm dishes in DMEM containing FCS (10%). The following morning, cells were transfected with 5 μg of plasmid encoding murine FLAG-NLRP3 (Addgene, 75127) using lipofectamine 2000. 24 h after transfection, cells were treated with 4-OI (250 μM) or vehicle control (DMSO) for a further 24 h. Following treatment, cells were washed with 3 mL PBS before lysis in 500 μL low stringency lysis buffer (50 mM HEPES pH 7.5, 100 mM NaCl, 1 mM EDTA, 10% glycerol, 0.5% Nonident P40 (NP-40), 1 mM phenylmethylsulfonyl fluoride (PMSF), 11.5 μg/mL aprotinin, 1 μg/mL leupeptin and 1 mM sodium orthovanadate) on ice. Plates were scraped with a cell scraper and lysate transferred into microcentrifuge tubes. Tubes were agitated at 1100 rpm at 4°C for 15 min before being centrifuged at 21380 x g for 10 min at 4°C. FLAG-tagged NLRP3 was immunoprecipitated using an anti-FLAG antibody (1 mg/mL, Sigma, F1804) and 70 μL A/G PLUS agarose beads (Santa Cruz), placed in a ferris wheel mixer at 4°C for 3 h. IP samples were subsequently centrifuged at 400 x g for 2 min at 4°C, supernatant removed, and beads washed three times with 1 mL low stringency lysis buffer. The immune complexes were eluted by addition of 40 μL sample lysis buffer, boiled for 5 min and run on a 8% gel. The resulting gel was subsequently fixed in Coomassie fixing solution (50% methanol, 10% acetic acid in ddH_2O) for 30 min, followed by removal of the fixing solution and incubation in Coomassie blue R-250 buffer (0.125 g Coomassie Blue R-250 (Cayman Chemical), 5 mL acetic acid, 22.5 mL methanol, 22.5 mL ddH_2O) for 1 h. Staining solution was then removed from the gel, which was washed repeatedly with de-staining solution (5% methanol, 7.5% acetic acid in ddH_2O). The corresponding bands for FLAG-NLRP3 were excised from the gel and subjected to in-gel digest with elastase (Promega). In brief, the gel slices were cut into smaller pieces (1–2 mm^3) before reduction with DTT (10 mM) and alkylation with iodoacetamide (50 mM). Gel slices were digested with elastase (1 μg) overnight at 37 °C. Following protease digest, peptides were eluted from the gel pieces and dried down completely in a vacuum centrifuge. Samples were analyzed in an Orbitrap Fusion Lumos coupled to a UPLC ultimate 3000 RSLCnano System (both Thermo Fisher). MS data was analyzed with PEAKS Studio 8 (Bioinformatics Solutions). Precursor mass tolerance was set to 10 ppm, while fragments were detected with a tolerance of 0.5 Da. Oxidation (M), Deamidation (N, Q), Carbamidomethylation (C), dicarboxypropylation of cysteine by 4-OI (C) (+242.15 Da) were defined as variable modifications. Peptide FDR was set to 1%.

MSU-Induced Peritonitis Model

6-week old female C57BL/6J mice were injected intraperitoneally with a mixture of 4-OI (50 mg/kg) in 60% cyclodextrin in PBS and MSU crystals (30mg/kg, Invivogen) suspended in PBS for 6 h. Mice were euthanized in a CO_2 chamber and peritoneal lavage was performed using 2.5 mL PBS. The cells in the lavage fluid were pelleted and the supernatant was removed and analyzed by ELISA for IL-1β and IL-6 concentration. Cells were resuspended in 1 mL PBS and passed through a 70 μm filter. 100 μL cells was removed for FACS analysis and the remaining cells were counted using a TC20™ automated cell counter (Biorad) with a minimum size gate of 8 μm and a maximum gate of 20 μm. 100 μL cells were incubated for 20 min at RT with Zombie Green (Biolegend, 1/800). Cells were then washed and incubated for 10 min at RT with anti-mouse CD16/CD32 (BD Biosciences) in 100 μL PBS. After 10 min, 1 μg of the following antibodies was added: APC/Cy7 anti-mouse CD45 (Biolegend), eFluor660 anti-mouse CD11b (ThermoFisher Scientific) and Pacific Blue anti-mouse Ly6G (Biolegend). After 20 min, cells were washed, resuspended in PBS and analyzed on a FACS Canto II Cell Analyzer (BD Biosciences). Neutrophils were identified as Zombie Green negative (live cells), $CD45^+CD11b^+Ly6G^+$ cells. Analysis of acquired data was performed with the FlowJo software (FlowJo LLC). The total number of neutrophils obtained from each mouse was calculated by multiplying the percentage neutrophils with the total cell count obtained.

QUANTIFICATION AND STATISTICAL ANALYSIS

Details of all statistical analyses performed can be found in the figure legends. Data were expressed as mean ± standard error of the mean (SEM) and p values were calculated using two-tailed Student's t test for pairwise comparison of variables and one-way ANOVA for multiple comparison of variables. A Sidak's multiple comparisons test was used as a post-test when performing an ANOVA. A confidence interval of 95% was used for all statistical tests. Statistical tests were not performed on western blot quantification figures due to the semiquantitative nature of these data. Significance was defined as follows: *$p < 0.05$, **$p < 0.01$, ***$p < 0.001$. Sample sizes

were determined on the basis of previous experiments using similar methodologies. All depicted data points are biological replicates taken from distinct samples. Each figure consists of a minimum of 3 independent experiments from multiple biological replicates. n = the number of animals or the number of independent experiments with cell lines. For *in vivo* studies, mice were randomly assigned to treatment groups. For mass spectrometry analyses, samples were processed in random order and experimenters were blinded to experimental conditions.